

Noncontact pulse wave detection by two-band infrared video-based measurement on face without visible lighting

Ryota Mitsuhashi^{*1}, Genki Okada^{*1}, Koki Kurita^{*2}, Keiichiro Kagawa^{*2}, Shoji Kawahito^{*2}, Chawan Koopipat^{*3} and Norimichi Tsumura^{*1}

¹Graduate School of Advanced Integration Science, Chiba University, 1-33 Yayoi-cho, Inage-Ku, Chiba 263-8522, Japan

²Research Institute of Electronics, Shizuoka University, Hamamatsu, Japan

³Department of Imaging and Printing Technology, Chulalongkorn University, Thailand
e-mail:r.mitsuhashi@chiba-u.jp

Abstract: In this paper, we propose a novel noncontact pulse wave monitoring method that is robust to fluctuations in illumination through use of two-band infrared video signals. Because the proposed method uses infrared light for illumination, the method can be used to detect a pulse wave on a human face without visible lighting. The corresponding two-band pixel values in the video signals can be separated into hemoglobin and shading components by application of a separation matrix in logarithmic space for the two pixel values. Because the shading component has been separated, the extracted hemoglobin component is then robust to fluctuations in the illumination. The pixel values in the region of interest (ROI) were spatially averaged over all the pixels of each frame. These averaged values were then used to form the raw trace signal. Finally, the pulse wave and the corresponding pulse rate were obtained from the raw trace signal through several signal processing stages, including detrending, use of an adaptive bandpass filter, and peak detection. We evaluated the absolute error rate for the pulse rate between the estimated value and the ground truth obtained using an electrocardiogram. In the experiments, we found that the performance of the proposed method was greatly improved compared with that of conventional methods using single-band infrared video.

Keywords: pulse wave, pulse rate, infrared, noncontact measurement

1 INTRODUCTION

Recently, noncontact methods have been proposed for physiological information measurement using video cameras. The pulse rate is one of the vital signs that are used to reflect the physiological health of humans, and it plays an important role in health care monitoring. Pulse rate monitoring can be used to monitor fatigue, concentration at work and drowsiness when driving, and can also help to prevent sudden infant death syndrome, heart attacks or paroxysmal diseases in patients located both at home and in the hospital.

Verkruysse et al. [1] found that the time-series variations of the pixel values in the region of interest (ROI) showed strong correlations with physiological information such as pulse rate. This is because the peak of spectral curves are matched between the oxy-hemoglobin and the green channel of the standard RGB camera. Therefore, the green channel showed the strongest features for extraction of physiological information. Poh et al. [2,3] developed a noncontact pulse wave monitoring method by using low cost webcam. Their method based on an application of independent component analysis to the variation of the spatially averaged pixel values in the ROI from standard RGB video recordings made under ambient light conditions. McDuff et al. [4] developed a noncontact method to estimate both the pulse wave and the patient's physiological status through a heart rate variability spectrogram (HRVS) measured using a five-band sensor

with red, green, blue, cyan, and orange (RGBCO) bands. They intended to use the five-band video recordings to estimate the patient's physiological status based on an heart rate variability spectrogram produced by an analysis of the R to R wave (RR) - intervals in the frequency domain. Kurita et al. [5] proposed a noncontact pulse wave monitoring method based on the extraction of hemoglobin information from standard RGB video recordings under ambient light conditions. They also intended to use the three-color channel signals to estimate the patient's physiological status via heart rate variability spectrogram in a visible light environment.

In the above applications, it may be necessary to measure the face at night without visible lighting while the subjects are driving or sleeping. Conventional RGB video recordings therefore cannot be used in such situations. Garbey et al. [6] proposed a method to measure pulse waves from single-band thermal video recordings of the subject's neck based on spatial averaging of the variations in the pixel values in the ROI. They performed experiments using a single-band mid-wavelength infrared video camera. However, their thermal imaging system required a specific camera and use of a differential blackbody as a calibration device. Zeng et al. [7] proposed a method to estimate the pulse rate based on the maximum of the power spectrum in the frequency domain using single-band infrared video recording. Hamedani et al.

[8] developed a method for pulse rate extraction using a 16-bit single-band thermal video camera. The pulse rate was obtained by magnifying the recorded thermal video using Eulerian video magnification and spatial-temporal filtering techniques. While the single-band video-based methods by using mid-wavelength infrared video[6], near infrared video [7], and thermal video [8] can detect the pulse rate without use of visible lighting, they cannot be used in situations where the illumination fluctuates as it does in real environments, such as the illumination when driving. Because the pixel values were affected by fluctuations in the illumination, the measurement results can thus also be affected. To solve this problem and enable implementation of these methods in the proposed applications, removal of the fluctuations arise from illumination is therefore essential.

De Haan et al. [9] aimed at robust pulse rate extraction by using infrared light. They conducted two experiments which one is using three-band monochrome camera with attaching bandpass filters and other is using RGB camera with attaching visible light blocking filter. Their pulse vector was determined by accurate measurement while considering the camera sensitivity, skin reflectance, and spectral distribution of illumination based on the study published in Hulsbusch et al. [10] and Correl et al. [11]. However, in case of three-band monochrome camera, they intended to use the bandpass filter of visible region around 640nm. This result implies that visible light for illumination can be occurred to disturb the person such like patients or driver when driving. Moreover, in case of RGB camera, they intended to require the visible light blocking filter and more specific LED light based on the use of the incandescent light. This result also implies that their experimental setup takes costs and not feasible in real environment. On the contrary, although we used artificial sunlight for illumination as an experimental setup, our result shows that the light for illumination is only required just two types of LEDs and both wavelength are invisible. Based on that, our proposed method is more suitable in real application for robust pulse rate extraction.

In this paper, we propose a noncontact pulse wave monitoring method that is robust to fluctuations in illumination based on the use of two-band infrared video signals. The two-band infrared video signals can be separated into hemoglobin and shading components by application of a separation matrix in logarithmic space. When the shading component has been separated, the extracted hemoglobin information will then be robust to fluctuations in the illumination. The pixel values of the ROI are spatially averaged over all the pixels in each frame. These

averaged pixel values are then used to form the raw trace signal. Finally, the pulse wave and the pulse rate are obtained from the raw trace signal via several signal processing stages, including detrending and adaptive bandpass filtering. In this work, we evaluate the absolute error rate (AER) for the pulse rate between the estimated value (EV) and the ground truth (GT), which was obtained using an electrocardiogram.

2 PROPOSED METHOD FOR ROBUST EXTRACTION OF PULSE WAVE FROM TWO-BAND INFRARED VIDEOS

In this section, we describe the procedure to obtain the pulse wave from the two-band infrared video signals. For the explanation provided in this section, we assume the use of a combination of bandpass filters with central wavelengths of 780 nm and 900 nm. These filters were attached at the front of each monochrome camera. Note this combination of filters is found in selection process described in Section 3.

Figure. 1(a) and (b) show the captured facial video recordings from the two-band camera at the central wavelengths of 780 nm and 900 nm, respectively. The corresponding two-band pixel values of each wavelength were converted into points in the color vector space, where each pixel value is converted into a logarithmic value, as shown in Fig. 2. The horizontal and vertical axes in Fig. 2 indicate the logarithmic pixel values in the two-band infrared videos. According to the study of Kurita et al. [5], they assumed the two-layered skin model based on the modified lambert-beer law. Similarly, we also applied the modified lambert-beer law into the single-layered model as we described on Fig. 5 (a), (b) in section 3. Here, we introduce a brief example of the process of conversion of the two-band infrared video signals into their hemoglobin and shading components in each frame. Assuming two dimensional plane constructed from the pixel values of two-band images corresponding to same location, (e.g. forehead), as shown in red point in Fig. 1(a),(b), respectively. An arbitrary vector \mathbf{A} is expressed as the linear combination of basis vector as shown in left term of the equation (1). Vector \mathbf{A} was also expressed as the linear combination of new basis vector in color space via logarithmic transformation as shown in Fig. 2. Therefore, vector \mathbf{A} can be expressed by two patterns as the following equation (1), respectively.

$$\mathbf{A} = I_1 \mathbf{e}_x + I_2 \mathbf{e}_y = I_1' \mathbf{e}_h + I_2' \mathbf{e}_s \quad (1)$$

Here, I_1 and I_2 are the logarithmic pixel values before the video signals were converted into their hemoglobin and

Figure 4(c) shows the pulse wave that was bandpass filtered using the adaptive window described above. Additionally, the pulse wave peaks were detected by calculating the maximum values of the signals every 15 frames. The RR intervals were calculated as the intervals between the neighboring peaks. Finally, Pulse rate was obtained by averaging these RR intervals as following equation.

$$PR = \frac{60}{RR \text{ intervals}} \quad (6)$$

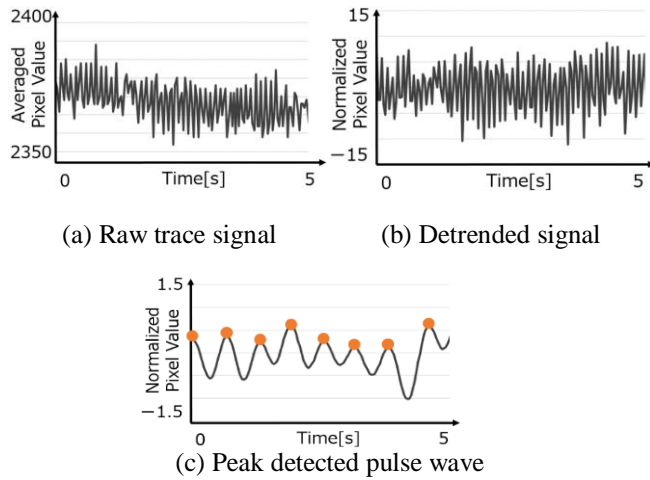


Fig. 4 Signal processing steps used to detect pulse wave

3 SELECTION OF EFFECTIVE TWO-BAND INFRARED FILTERS

Kurita et al. [5] used a two-layer skin model composed of the epidermis and the dermis. They simplified the model by assuming the epidermis only contained chromophores of melanin, and the dermis only contained chromospheres of hemoglobin. Their experiments were conducted under ambient light using an RGB camera. Because the visible light is absorbed and reflected by the layers of the epidermis and the dermis, a two-layered skin model is used, as shown in Fig. 5(a). However, in this paper, we used a single-layer skin model, as shown in Fig. 5(b), because the infrared light is only absorbed and reflected by the dermis. The penetration depth of the invisible (infrared) light is deeper than visible light because the wavelength of the infrared light is longer than the visible light. The pulse wave was then obtained by extracting the hemoglobin information after converting two-band infrared video signals into decomposed video signals, as described in previous section. In this process, it is necessary to find an effective combination of the two-band infrared wavelengths that allows sufficient variation of the

hemoglobin component to be captured. We simulated some combinations of the bandpass filters while considering the relationships among the reflectance of the oxy-hemoglobin, the sensitivity of the monochrome camera, and the spectral curves of the bandpass filters, as shown in Fig. 6(a), (b) and (c). We used the bandpass filters with central wavelengths of 780 nm, 820 nm, 860 nm, 900 nm, and 940 nm and a full width at half maximum of ± 10 nm, in each case (Edmund Optics Japan Inc.). First, Fig. 6 (a) indicates that the density of oxy-hemoglobin increases at higher wavelength. So that, the combinations of wavelengths of bandpass filters should be far from each other since the difference of the absorbance characteristics can be obtained from each wavelength. On the other hand, Fig. 6 (b) indicates that the sensitivity of the monochrome camera decreases at higher wavelength. Therefore, we have to choose the wavelengths with considering the difference of the absorbance characteristics in oxy-hemoglobin while keeping camera sensitivity. In order to verify the combinations with considering the above relationships, we prepared the five band-pass filters in infrared region which central wavelengths are range of from 780nm to 940nm as shown in Fig. 6 (c). Therefore, the effective two-band infrared video signals can obtain sufficient variation in the oxy-hemoglobin easily than a single-band infrared video signals. Based on these scenarios, the most effective combination of the bandpass filters was determined based on this tradeoff relationships between the absorbance of the oxy-hemoglobin and the sensitivity of monochrome camera as shown in Fig. 6(a), (b) and (c).

We simulated the experiment using the following steps to capture the variation of the oxy-hemoglobin. First, we calculated the reflectance of the skin to be close to the real skin. Second, the pixel values were calculated by integrating the skin's reflectance, the sensitivity of the monochrome camera, and the spectral curves of the bandpass filters. Third, the pixel values were separated into their hemoglobin and shading components. Finally, we evaluated the separated components using the evaluation function and obtained an effective combination of bandpass filters that could capture sufficient variation in the oxy-hemoglobin.

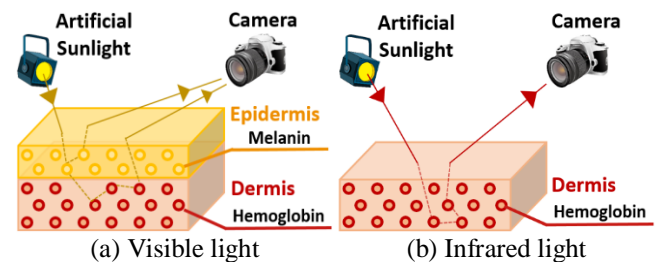


Fig. 5 Layered skin model at different light wavelengths

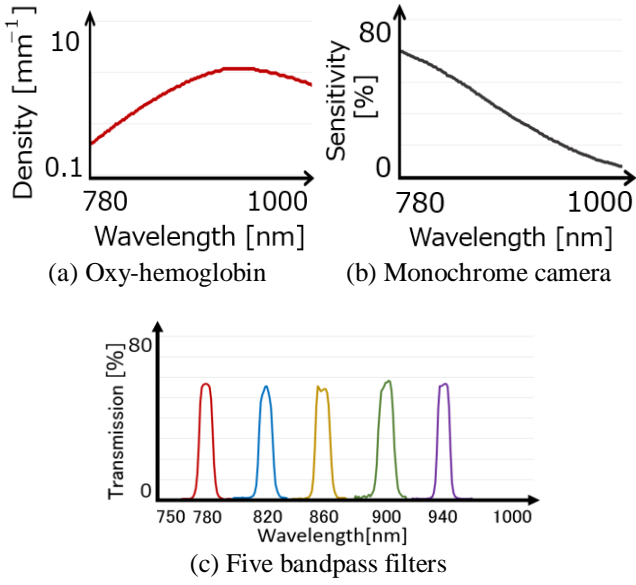


Fig. 6 Spectral curves used to simulate the effective combinations of the bandpass filters

The hemoglobin components are distributed all over the skin by blood circulation. In this paper, we assumed a situation where the oxy-hemoglobin density values were distributed to each pixel value with different densities. We calculated the oxy-hemoglobin distribution as a range from 0.200 to 0.213 cm^2/mol with 100 steps to be close to the reflectance on a real face. In addition, the density of the oxy-hemoglobin in a blood vessel is slightly increased by the enlargement of the vessel caused by the heartbeat. As the first step in our study, we calculated the variation in the oxy-hemoglobin caused by a heartbeat over a range from 0.00000 to 0.00068 cm^2/mol with two steps to be close to the reflectance on a real face. The reflectance of the virtual skin was then calculated based on these parameters using the following equation, and the simple virtual skin model was simulated for selection of the most effective combination of two-band infrared filters.

$$R(\lambda) = \exp(-aD(\lambda)) \quad (7)$$

where $R(\lambda)$ is the reflectance of the skin model, a is the amount of the variation in the oxy-hemoglobin and $D(\lambda)$ is the density of the oxy-hemoglobin. The pixel values that were obtained from the skin model were given by integrating each component as shown in the following equation.

$$I = \int sR(\lambda)C(\lambda)B(\lambda) d\lambda \quad (8)$$

Where $C(\lambda)$ represents the sensitivity of the monochrome camera, $B(\lambda)$ represents the spectral curves for each of the bandpass filters, s is the shading factor, and λ is the wavelength. We assumed that the illumination intensity is constant in this work. To match the bit depth of the experimental setup, the pixel values of the two-band infrared video signals were calculated via an 8-bit quantization process in the simulations. The oxy-hemoglobin component was estimated by determining the new basis vector in the color vector space constructed from the pixel values of the two-band infrared video recordings. The corresponding two pixel values were converted into the color vector space by taking logarithm of these values. The actual pixel values include the dark current noise, which heavily affects the estimation of the pulse rate. In this paper, we simulated the dark current noise by assuming a Gaussian distribution. We evaluated the most effective combinations of the filters to capture the oxy-hemoglobin variation using a following equation.

$$E = \frac{|I_{h+\Delta h} - I_h|^2}{V_{h+\Delta h} \cdot V_h} \quad (9)$$

Here, I_h and V_h represent the pixel values and the variance of these pixel values before the oxy-hemoglobin density was varied from the specified density level, respectively. $I_{h+\Delta h}$ and $V_{h+\Delta h}$ also represent the pixel values and the variance of the pixel values after the oxy-hemoglobin density was varied from the specified level. The evaluated value was close to zero when the variation in the oxy-hemoglobin was not captured due to an increase of the dark current noise. Therefore, the set of the filters that gives the highest evaluation value despite the increased noise was determined to be the most effective combination for easier detection of the pulse wave and the pulse rate in this paper. As a result of these simulations, evaluation curves for each of the combination were obtained as shown in Fig. 7.

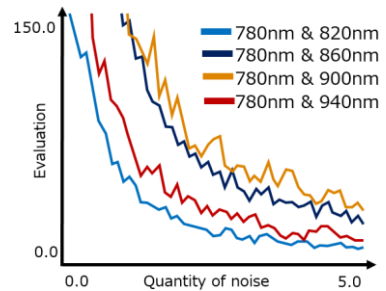


Fig. 7 Evaluation curves for each combination of filters using the evaluated function shown in Eq.(8)

The combinations of filters with wavelengths that were close to each other were strongly affected by the random noise, even if there was only a slight amount of noise. Combinations of filters with wavelengths that were far apart from each other tended to be more robust to the random noise. However, the combination with wavelengths of 780 nm and 940 nm received a poor evaluation because of the low sensitivity of the camera around 1000 nm, as shown in Fig. 6(b). In case of the wavelengths of 780nm and 900nm, the higher evaluation values are kept in presented combinations despite an increase of noise. Therefore, as shown in the evaluation curves, a filter combination with wavelengths of 780 nm and 900 nm was selected as the most effective combination for capture of the variations in the oxy-hemoglobin in this work.

4 EXPERIMENTAL SETUP

The experiments were performed indoors in a dark room with two artificial sunlight lamps acting as sources of illumination, as shown in Fig. 8. In this work, the flickering of the artificial sunlight played the role of the fluctuation in the light source environment. Participants were seated in front of a table and fixed in position using a thin rest positioned in front of the two-band camera at distances of approximately 0.5 m from the camera and 0.3 m from each artificial sunlight source. The two-band camera system is composed of a beam splitter and monochrome cameras, where bandpass filters are attached in front of each camera. As mentioned in section 3, filters with central wavelengths of 780nm and 900nm were selected as the most effective combination to capture the variations in the oxy-hemoglobin. Therefore, we limited the incident light to the monochrome camera with the central wavelength of 780 nm and a full width at half maximum of ± 10 nm. We also limited the incident light to the other monochrome camera in the range in which the central wavelength is 900 nm with a full width at half maximum of ± 10 nm. During the experiments, participants were asked to remain as still as possible and to breathe spontaneously. Additionally, the participants were also asked to face the two-band camera while their videos were recorded for 2 mins. We recorded these videos using the following two patterns. The first video was recorded without fluctuations in the illumination using artificial sunlight under stable conditions. The stable artificial sunlight condition can be obtained by waiting for more than 30 min after the start of lighting. The second video was recorded under conditions with fluctuations in the illumination using the artificial sunlight. These illumination fluctuations can be observed if the artificial sunlight source is turned up in less

a minute. We conducted this experiment by assuming that the former was an environment without illumination fluctuations and the latter was an environment with illumination fluctuation. All videos were recorded using an 8-bit monochrome camera at 30 fps with pixel resolution of 640×480 and were saved in BMP format on a personal computer.

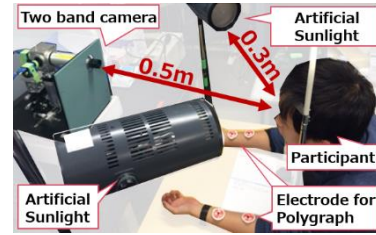


Fig. 8 Two-band infrared videos were obtained by recording the light reflectance from the participant's skin

We also recorded an electrocardiogram for participant using a polygraph system at a sampling rate of 1 kHz with a cut-off frequency of 15 Hz (RMT1000; Nihon Kohden Inc.). The ground truth of the heart rate was calculated by averaging RR intervals obtained from the electrocardiogram for verification of the proposed method's accuracy.

5 EXPERIMENTAL RESULTS

We evaluated the estimated pulse rate using our method based on the absolute error rate (*AER*), as given in the following evaluation equation.

$$AER = \frac{|GT - EV|}{GT} \times 100 \quad (10)$$

Here, *GT* represents the ground truth that was obtained via the electrocardiogram. *EV* represents the estimated value determined using our proposed method. The *AER* between the estimated value and the ground truth is normalized with respect to the ground truth. This gives an indication of how close the estimated value is to the ground truth.

The raw trace signals in the two infrared bands and signal processing steps are shown in Fig. 9. Table 1 shows the profile comparing the estimated pulse rate with the ground truth without fluctuation of illumination. According to Table 1, the *AER* of the pulse rate when using the two-band infrared video signals shows higher accuracy when compared with the method using the single-band infrared video [6]. Table 2 shows the profile of results when comparing the estimates of the pulse rate and the ground truth with varying illumination. We confirmed from these results that the pulse

rate estimates were strongly affected by the fluctuations in the illumination. The results obtained using the proposed method also show that our method provides greatly improved performance when compared with that of the conventional method because the corresponding pixel values of the videos have been separated into the hemoglobin and shading components by fixing the fluctuation of illumination (shading) to the (1, 1) vector in the color vector space.

6 DISCUSSION

As we mentioned with regard to the results of our experiment, we estimated the pulse rate in an environment without visible lighting with higher accuracy than the conventional method based on noncontact pulse wave monitoring using a single-band infrared video camera [7]. In particular, our method worked well even in the case where there were fluctuations in the illumination through use of the effective combination of the two-band infrared filters.

As we described in Section 1, the method using single-band infrared video camera was obtained by calculating the spatially averaged pixel values within the ROI [7]. The pulse rate was then estimated via a frequency analysis. The *AER* accuracy of single-band near infrared video showed less than 1% without illumination fluctuation.

According to the results in Table 1, we obtained *AER* values of 8.17% and 6.98% for the estimated pulse rate when using the single-band video only. We consider that these results can be attributed to several reasons. First, the raw trace signal was suspected to be heavily affected by the low sensitivities of the monochrome camera and dark current noise and random pattern noise because we used the beam splitter and narrow bandpass filters which band range is only 20 nm as the experimental setup.

Second, The ROI without tracking were captured at slightly different places in each frame. Despite the fact that the participant's faces were fixed to the thin rest and the ROI of the forehead was set, the participants moved slightly during the continuous 2mins recording. In fact, the accuracy can be improved by implementing facial tracking or mask processing of the face region during the video recording step. We considered the possibility that the raw trace signal was affected by these tiny movements and thus the pulse rate was also affected by these factors. The results in Table 2 confirmed that single-band infrared video could not be used to obtain the pulse rate with sufficient accuracy when there were fluctuations in the illumination because the *AER* values of the pulse rates measured using only single-band infrared video showed poor performance, with accuracies of 18.66% and 29.56%. We considered that the bandpass filter did not

sufficiently remove the fluctuations in the illumination due to the aperiodic noise. Therefore, the noise frequency was included within the frequency range of the bandpass filter and the pulse rate was affected by the inclusion of the noise.

We obtained *AER* values for the pulse rate with accuracy of 0.45% without illumination fluctuations and 3.73% with illumination fluctuations. These results indicate the robustness of the proposed method using two-band infrared video signals to illumination fluctuations because the videos are separated into the hemoglobin and shading components by the proposed application of the basis translation matrix in the color vector space. As mentioned earlier, higher accuracy can be obtained by implementing facial tracking or mask processing of the face region. To enable further discussion of the factors affecting the *AER*, the distributions of the pixel values were obtained after the translation matrix was applied in logarithmic space as shown in Fig. 10. These figures show that the pixel values recorded using the two-band infrared camera can be decomposed into the shading and hemoglobin components in logarithmic space. We then selected the hemoglobin vector as the optimal vector for pulse rate estimation with the highest accuracy across whole vector range of from 0° to 90° . However, we obtained results with low accuracy when compared with the results from the method by using single-band near infrared video. As shown in Fig. 3 (a), the hemoglobin vector may be determined incorrectly because, in hemoglobin image, shading component was observed around the nose. However, we obtained the effective hemoglobin vector in the case of with illumination fluctuation. Therefore, we must try to decompose the video signals using the hemoglobin vector in the case of without illumination fluctuation.

Table 1 Comparison of the ground truth with the estimated pulse rate in each single-band without variation in the illumination. *GT*: ground truth; *EV* estimated value; *AER*: absolute error rate

	<i>GT</i> [bpm]	<i>EV</i> [bpm]	<i>AER</i> [%]
One band 780nm	89.12	96.46	8.17
One band 900nm	89.12	95.40	6.98
Two band 780nm, 900nm	89.12	88.77	0.45

Table 2 Comparison of the ground truth with the estimated pulse rate in each single-band with variation in the illumination. *GT*: ground truth; *EV*: estimated value; *AER*: absolute error rate

	<i>GT</i> [bpm]	<i>EV</i> [bpm]	<i>AER</i> [%]
One band 780nm	98.94	117.40	18.66
One band 900nm	98.94	69.69	29.56
Two band 780nm, 900nm	98.94	102.63	3.73

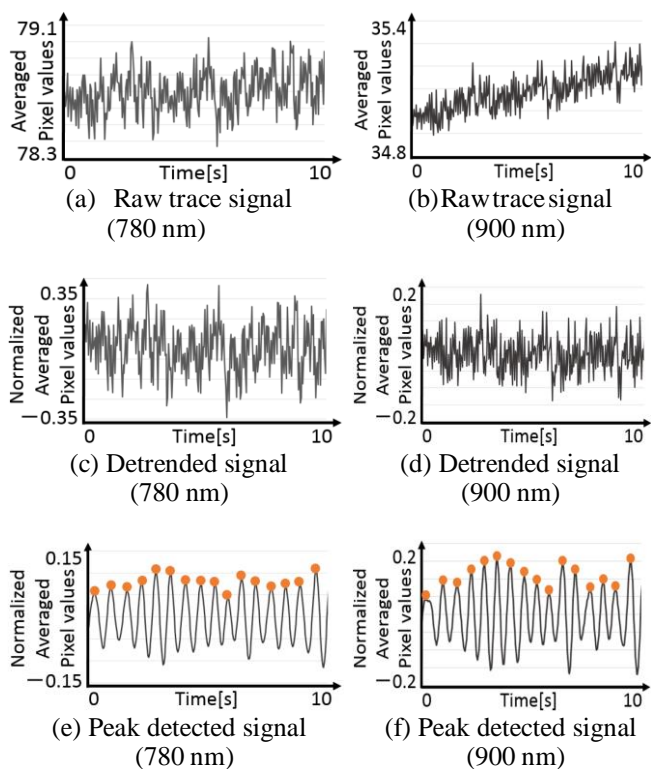


Fig. 9 Signal processing steps used to detect the pulse wave from single-band infrared video signal

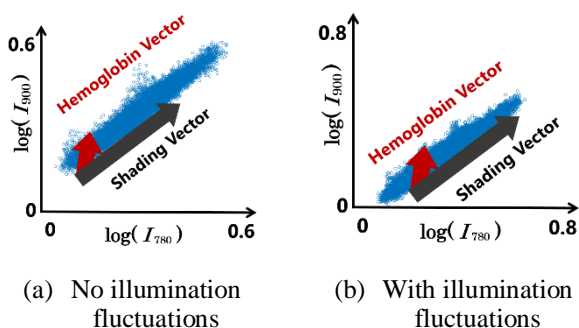


Fig. 10 Distributions of the pixel values in logarithmic space and the directions of the hemoglobin vector and the shading vector

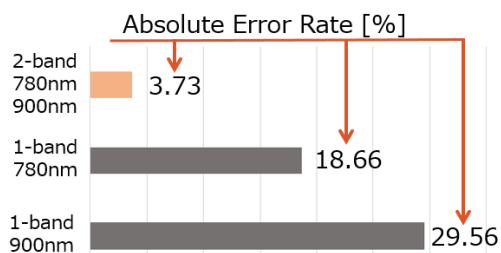


Fig. 11 Comparison of the AERs in the single-band and two-band cases

7 CONCLUSIONS AND FUTURE WORK

We proposed a noncontact pulse wave monitoring method that is robust to illumination fluctuations. Separated hemoglobin and shading components were obtained by determining a new basis vector in the color vector space. As shown in Fig. 11, our proposed method showed greatly improved accuracy, with an improvement from 29.56% to 3.73% when compared with the results of the conventional method that used single-band infrared video signal [7].

In order to verify the effectiveness of our method, large number of subjects will be needed as one of our future works. It will be necessary to improve the accuracy of pulse rate estimation using the proposed method by implementing facial tracking. We obtained the optimal hemoglobin vector in the case with illumination fluctuations. We therefore need to try to estimate the pulse rate using the optimal hemoglobin vector in the case without illumination fluctuations and then decompose the videos using obtained hemoglobin vector. By implementing these improvements, we will attempt to measure the pulse rate variability, which is robust against illumination fluctuations, using a two-band infrared camera system without use of visible light sources in our future work.

ACKNOWLEDGEMENTS

This work was supported in part by the MEXT/JST COI STREAM program.

REFERENCES

- [1] W. Verkruijse, L. O. Svaasand and J. S. Nelson, "Remote plethysmographic imaging using ambient light," *Opt. Exp.*, vol. 16, no. 26, pp. 21434-21445, (2008).
- [2] M. Z. Poh, D. J. McDuff, and R. W. Picard, "Non-contact, automated cardiac pulse measurements using video imaging and blind source separation," *Opt. Exp.*, vol. 18, no. 10, pp.10762-10774, May 2010.
- [3] M. Z. Poh, D. J. McDuff, and R. W. Picard, "Advancements in noncontact, multiparameter physiological measurements using a webcam," *IEEE Trans. Biomed. Eng.*, vol. 58, no. 1, pp. 7-11, Jan. 2011.
- [4] D. McDuff, S. Gontarek, R. W. Picard, "Improvements in Remote Cardio-Pulmonary Measurement Using a Five Band Digital Camera" *IEEE Transactions on Biomedical Engineering*, pp. 2593-2601, (2014).
- [5] Kurita K, Yonezawa T, Kuroshima M and Tsumura N, "Non-Contact Video Based Estimation for Heart Rate Variability Spectrogram using Ambient Light by Extracting Hemoglobin Information," *Color and Imaging Conference*, Volume 2015, Number 1, October 2015, pp. 207-211
- [6] M. Garbey, N. Sun, A. Merla, and I. Pavlidis, "Contact-free measurement of cardiac pulse based on the analysis of thermal imagery," *IEEE Trans. Biomed. Eng.*, vol. 54, no. 8, pp. 1418-1426, Aug. 2007
- [7] Wei Zeng, Qi Zhang, Yimin Zhou, Guoqing Xu, Guoyuan Liang. "Infrared Video based Non-Invasive Heart Rate Measurement".

IEEE Conference on Robotics and Biomimetics, December 6-9, 2015, pp. 1041-104

[8] K. Hamedani, A. Veeraraghanvan, and A. Sabharwal, "Spatio-temporal filtering of thermal video sequences for heart rate," Elsevier, Expert Systems with Applications, no. 54, pp. 88-94, 2016

[9] Van Gastel, S. Stuijk, De Haan, "Motion Robust Remote-PPG in Infrared", IEEE Transactions on bioengineering, vol. 62, no. 5, pp.1425-1433, MAY 2015

[10] M. Hulsbusch, "An image-based functional methodfor optoelectronic detection of skin-perfusion (in German)," Ph.D. dissertation, RWTH Aachen, Aachen, Germany, 2008

[11] L. F. Corral, G. Paez and M.Strojnik, "Optimal wavelength selection for non-contact reflection photoplethysmography", 22nd Congress of the International Comission for Optics, Puebla, Mexico, Proc. SPIE vol. 8011, 8011-91, 15-19 Aug.(2011)

[12] M. P. Tarvainen, P. O. Ranta-aho, and P. A. Karjalainen, "An advanced detrending method with application to hrv analysis," Biomedical Engineering, IEEE Transactions on, vol. 49, no. 2, pp. 172-175, 2002